THE JOURNAL OF PHYSICAL CHEMISTRY A

 VOLUME 105, NUMBER 37, SEPTEMBER 20, 2001

ARTICLES

Resonance Raman and ab Initio Studies of the Electronic Transitions of Aqueous Azide Anion

Mark R. Waterland[†] and Anne Myers Kelley*

Department of Chemistry, Kansas State University, Manhattan, Kansas 66506-3701

Received: March 12, 2001; In Final Form: June 26, 2001

Resonance Raman spectra and absolute cross sections have been measured for the azide anion (N_3^-) in dilute aqueous solution at excitation wavelengths of 246, 228, 223, 218, and 208 nm, on resonance with the longest-wavelength UV absorption bands. The spectra are dominated by the fundamental of the 1343 cm^{-1} symmetric stretch, with much lower intensities in the first overtone of the symmetric stretch and the overtone of the bending mode at 1275 cm^{-1}. The weak overtones and generally low resonance Raman cross sections suggest unusually small changes in the N−N bond lengths relative to those expected for valence transitions of small molecules, and/or particularly strong coupling of the electronic transitions to solvent degrees of freedom leading to rapid effective electronic dephasing. Ab initio calculations have been performed on complexes of N_3^- with three and four water molecules at the single CI level using the 6-311++g** basis with additional diffuse functions on the N atoms. These calculations predict that the low-lying dipole-allowed electronic excitations have large contributions from rather diffuse upper orbitals, and the forces on the atoms upon vertical excitation are mainly along azide-water and water−water intermolecular coordinates rather than internal vibrations of the azide. The experimental and computational results together are most consistent with significant charge-transfer-to-solvent precursor character of the resonant electronic state(s).

1. Introduction

Changes in the energies, band shapes, and/or intensities of electronic transitions resulting from solvation are the rule rather than the exception in molecular spectroscopy. Usually the perturbations to the spectra are relatively small and the electronic transitions are not substantially altered in character. Common exceptions include small anions in polar solvents, where the low-lying electronic transitions may include states that formally correspond to a photoinduced transfer of the excess electron from the anion to the solvent. These charge-transfer-to-solvent (CTTS) states have been known for a long time (see the comprehensive review by Blandamer and Fox[1]) but there has recently been renewed interest in both the energetics and, particularly, the dynamics of such transitions.[2−7] Much of the recent experimental and theoretical work has focused on solvated monatomic anions, generally halides. Diatomic and small polyatomic molecular anions can also exhibit CTTS transitions, but these are often more difficult to characterize and have been studied less extensively.

The azide ion (N_3^-) is one such molecular anion whose UV absorption spectrum in solution has been attributed in part to CTTS transitions. Thin films of alkali metal azides (e.g. KN_3) exhibit a fairly strong, unstructured absorption band with a maximum at about 190 nm, and a weaker, slightly structured absorption with a maximum near 225 nm.[8] A weak fluorescence with a maximum near 480 nm was also observed.[8] Burak and

* To whom correspondence should be addressed. Electronic mail: amkelley@ksu.edu.

[†] Current address: Department of Chemistry, Southwest Missouri State University, 901 S. National Ave., Springfield, MO 65804-0089.

10.1021/jp010925g CCC: $20.00
Published on Web 08/28/2001

Treinin carried out a detailed study of the absorption spectrum from 190 to 265 nm as a function of solvent, temperature, and added electron acceptor (I_2).[9] They concluded that the lowest-energy transition, observed only as a weak shoulder near 230 nm in room-temperature aqueous solution, probably originates from a valence transition localized on the azide ion ($^1\Delta_u \leftarrow {}^1\Sigma_g^+$) which involves a shift of charge from the terminal atoms toward the central atom, and corresponds to a transition from the linear ground state to a highly bent excited state. The stronger, higher-energy band, exhibiting a maximum near 190 nm in water, was assigned to overlapping contributions from an intramolecular electronic transition ($^1\Sigma_u \leftarrow {}^1\Sigma_g^+$) and a CTTS state. Subsequent workers, however, ignored or downplayed the importance of possible CTTS states, perhaps because their assignments, made with the aid of quantum chemical calculations on the bare anion, could not consider such transitions. Closson and Gray[10] agreed with Burak and Treinin's assignments for the internal transitions but made no reference to a CTTS state. McDonald et al.[11] concluded that the ~225-nm band (oscillator strength ~0.02 in aqueous solution) arises from the $^1\Sigma_u \leftarrow {}^1\Sigma_g^+$ transition, while the ~190-nm band ($f \sim 0.5$) is the $^1\Delta_u \leftarrow {}^1\Sigma_g^+$ transition. They suggested that a CTTS transition may underlie one or both of these bands and/or confer additional intensity on the $^1\Sigma_u \leftarrow {}^1\Sigma_g^+$ transition, but that the main features of the spectrum are adequately explained without consideration of CTTS states. Rossi and Bartram[12] supported McDonald's previous assignments of the UV transitions. They also calculated the triplet states of bent N_3^- and remeasured the low-temperature fluorescence spectra of solid KN_3,[13] and concluded that the fluorescence probably arises from a triplet−triplet transition. More recently, the ground-state vibrational dynamics of N_3^- in solution have been studied in detail through ultrafast time-resolved infrared spectroscopy and complementary molecular dynamics simulations.[14−17]

This paper reports and analyzes the far-UV resonance Raman spectrum, including absolute cross sections, of N_3^- in dilute aqueous solution. Previous Raman studies of N_3^- have been limited mainly to work on solid salts and the ion bound to heme proteins, although a nonresonant Raman study of aqueous N_3^- has been published.[18] The information about excited-state potential energy surfaces and dynamics contained in resonance Raman intensities has been utilized to deduce the properties of excited electronic states in a wide variety of molecular systems, including those that involve charge transfer between donor and acceptor moieties that are either covalently or noncovalently attached.[19−26] We do not know of any clearly assigned CTTS transitions for which resonance Raman data have been reported, and there is no unique experimental signature for resonance with a CTTS state. However, we expect that the delocalization of the electronic transition onto solvent molecules will tend to reduce the magnitude of the geometry change in the molecular coordinates relative to that expected for a localized transition, much as the change in the C=C bond length upon excitation of 1-aza-adamantane-4-ylidenemalononitrile is greater for the locally excited $\pi \rightarrow \pi^*$ transition than for the intramolecular charge-transfer transition.[27,28] Solvent or intermolecular vibrations might also be resonance enhanced in a CTTS transition. More likely, if the relevant modes are too low in frequency, heavily damped, or inhomogeneously broadened to appear as defined Raman lines, the coupling of the electronic transition to solvent motions will simply appear as an increase in the effective electronic dephasing rate. All of these factors should tend to reduce the resonance Raman intensity in the molecular modes of the azide ion (e.g. the symmetric stretch and its overtones) relative to that expected for a localized electronic transition.

2. Experimental Methods

The experimental setup was essentially the same as that employed in our recent UV resonance Raman studies of nitrate ion in solution.[29] Sodium azide (Acros Organics) was used as received, and 50-mM solutions were prepared by weight in distilled water. The Raman scattering was collected with reflective optics in a backscattering geometry from an open flowing jet, dispersed with a 0.75-meter single spectrograph, and detected with an intensified diode array. A 1200 groove/mm ruled grating blazed at 300 nm was used in first order with an entrance slit width of 150 μm, providing a spectral resolution of 20−30 cm^{-1} depending on excitation wavelength. Spectra were corrected for the wavelength dependence of the collection and detection system and for reabsorption of the scattered light, and integrated band areas were obtained by fitting regions of the spectra to sums of mixed Gaussian−Lorentzian peaks plus a linear background. Absolute differential Raman cross sections were determined relative to the OH-stretching band of water as an internal standard.[29,30]

3. Computational Methods

The electronic structure calculations were performed with the Gaussian 98 package. Geometry optimizations and vibrational frequency calculations on the ground states of bare azide and several azide-water complexes were performed at the RHF level. The 6-311++g** basis set was employed to provide the diffuse and polarization functions needed to describe molecular anions accurately. To model electronically excited states that may correspond to dipole-bound states with the electron in a highly diffuse orbital, the basis set was augmented[5] by adding four more diffuse sp shells on each nitrogen atom with orbital exponents of 0.2, 0.04, 0.008, and 0.0016, respectively. All of the reported structures have all-real vibrational frequencies and therefore correspond to local energy minima, although we cannot exclude the possibility that structures of lower energy exist. Vibrational frequencies were uniformly scaled by the recommended factor of 0.893 to compensate for neglect of electron correlation at the Hartree−Fock level.

Vertical excitation energies, transition dipole moments, and oscillator strengths were calculated using the CIS method at the optimized ground-state geometries. The derivatives of the excited-state potential energy with respect to the vibrational coordinates at the ground-state geometry were then calculated for selected low-lying excited states. The conversion between Cartesian and normal coordinates was calculated as discussed in our previous work on the nitrate ion.[31]

The resonance Raman intensity calculations were carried out using the time-dependent wave packet method, assuming contributions from two resonant electronic states having arbitrary relative polarizations, and harmonic vibrations with possibly different ground- and excited-state frequencies.[20,21,27,29,32] The differential Raman cross section is given by[27]

$$\left(\frac{d\sigma}{d\Omega}\right)_{||+\perp} = \sum_i B_i \sum_f \int d\omega_S \left(\frac{\omega_S{}^3 \omega_L}{c^4} \int d\delta G(\delta) a_{if}{}^{tot}(\omega_L,\delta)\right) \times L_{if}(\omega_L - \omega_S) \quad (1)$$

with

$$a_{if}^{tot}(\omega_L,\delta) = \frac{4}{15}\{|\alpha_1|^2 + |\alpha_2|^2 + \frac{1}{8}(\alpha_1^*\alpha_2 + \alpha_2^*\alpha_1)(7\cos^2\theta + 1)\} \quad (2)$$

where ω_L and ω_S are the laser and scattered frequencies, c is the speed of light, B_i is the thermal Boltzmann population of initial vibrational state $|i\rangle$, $L_{if}(\omega_L - \omega_S)$ is the line shape of the $|i\rangle \rightarrow |f\rangle$ vibrational transition, and the sums incorporate the contributions to the intensity from all $|i\rangle \rightarrow |f\rangle$ transitions that fall within a chosen range of scattered frequencies. $G(\delta)$ is a normalized static inhomogeneous distribution of electronic zero−zero energies taken to be a Gaussian; here the shifts of the two electronic states were assumed to be completely correlated (i.e., each local environment shifts both states by the same amount), which is the simplest assumption to make in the absence of any other information. θ is the angle between the transition dipole moment directions for the two electronic states. The contribution to the Raman amplitude from state k is given by

$$\alpha_k = \frac{|\mu_{k0}|^2}{\hbar}\int_0^\infty dt\langle f|i^k(t)\rangle \exp[i(\omega_L - \omega_k - \delta + \omega_i)t - g_k(t)] \quad (3)$$

where μ_{k0} is the transition dipole moment, ω_k is the electronic zero-zero frequency, ω_i is the frequency of initial state $|i\rangle$, and $g_k(t)$ is the solvent homogeneous broadening function, here taken to be a single overdamped Brownian oscillator as described in refs 33 and 34. The quantity $|i^k(t)\rangle$ is $\exp(-iH^kt/\hbar)|i\rangle$, the initial vibrational wave function propagated for time t on the potential surface for excited state k. The corresponding expression for the absorption spectrum is where n is the solvent refractive index

$$\sigma_A(\omega) = \sum_{k=1}^{2}\frac{4\pi\omega|\mu_{k0}|^2}{3n\hbar c}\sum_i B_i \int d\delta G(\delta) \times \mathrm{Re}\int_0^\infty dt\langle i|i^k(t)\rangle \exp[i(\omega - \omega_k - \delta + \omega_i)t - g_k(t)] \quad (4)$$

and Re represents the real part of the integral.

The experimental ground-state vibrational frequencies for azide were retained, while the scaled ab initio frequencies were used for the water vibrations and intermolecular modes. The excited-state potential parameters, transition moments, and electronic excitation energies were initially taken from the ab initio calculations and adjusted as needed to better fit the experimental resonance Raman intensities. The Brownian oscillator homogeneous broadening function is assumed to account for reorganization of solvent molecules not explicitly included in the ab initio calculations. For each complex, the absorption spectrum and Raman excitation profiles were calculated as a Boltzmann-weighted sum of 27 initial states ($n = 0$, 1, and 2 in each of the three lowest-frequency Franck−Condon active vibrations).

4. Results

Figure 1 shows the optical absorption spectrum of sodium azide in water and indicates the wavelengths at which resonance Raman spectra were obtained. Figure 2 presents the resonance Raman spectra at excitation wavelengths of 246, 228, 223, 218, and 208 nm. Apart from the broad water features, the spectra are dominated by the fundamental of the symmetric stretch (ν_1)

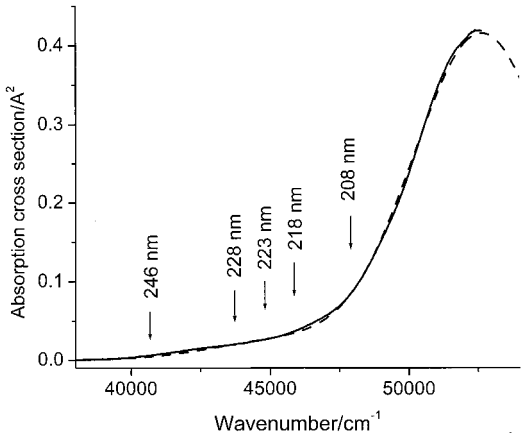

Figure 1. Optical absorption spectrum of NaN_3 in water (solid curve) and spectrum calculated from eq 4 and the refined parameters of Table 5 (dashed curve). The arrows indicate the five excitation frequencies at which resonance Raman spectra were obtained.

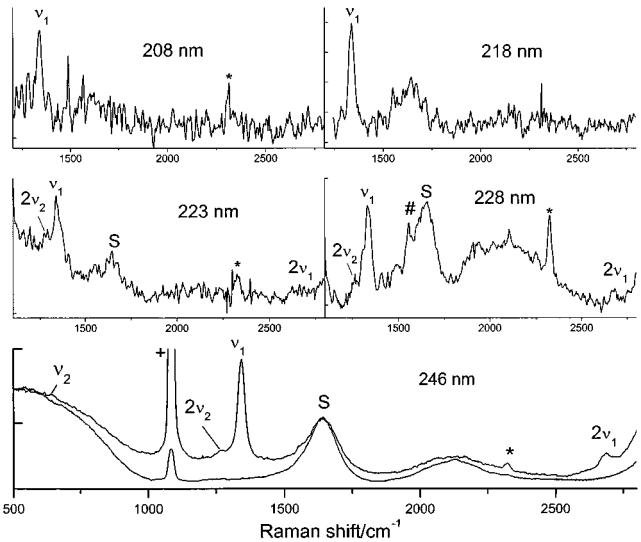

Figure 2. Resonance Raman spectra of 50 mM NaN_3 in water at the indicated excitation wavelengths. The pure solvent spectrum is shown as the dashed curve in the 246 nm spectrum. The Raman lines of N_3^- are labeled. The symbols +, #, and * label features resulting from stray laser lines and to Raman scattering from atmospheric O_2 and N_2, respectively.

at 1343 cm^{-1}. The symmetric stretch overtone at 2682 cm^{-1} is about an order of magnitude weaker than the fundamental with 246−223 nm excitation, and could not be clearly observed at all in the lower signal-to-noise spectra at 218 and 208 nm. The overtone of the bending vibration ($2\nu_2$) appears as a weak band at 1275 cm^{-1} in the 246−223 nm spectra. There is a hint of the bending fundamental as an extremely weak feature on top of the broad water band near 500 cm^{-1} in the 246 nm spectrum, but no measurable intensity in the fundamental of the antisymmetric stretch (ν_3), expected near 2049 cm^{-1}. Both of these transitions are nominally Raman forbidden for the symmetric linear ion but could become allowed due to local symmetry breaking as is the antisymmetric stretch of I_3^-.[35] Although the absolute scattering cross sections for the azide modes increase as the excitation is tuned to shorter wavelengths, the signal-to-noise ratio deteriorates severely because of reduced laser power, greatly increased absorption of both the incident and the Raman-scattered light, and decreased detection efficiency. We were not able to obtain useful spectra at 204 or 200 nm. Table 1

TABLE 1: Raman Cross Sections for NaN_3 in Water[a,b]

		$(d\sigma/d\Omega)/(10^{-11}$ Å^2 molecule^{-1} sr^{-1})					
		ν_1 (1343 cm^{-1})		$2\nu_1$ (2682 cm^{-1})		$2\nu_2$ (1275 cm^{-1})	
λ_{ex}/nm	cm^{-1}	expt	calc	expt	calc	expt	calc
246	40660	0.71	0.46	0.078	0.034	0.041	0.029
228	43727	1.1	2.7	0.11	0.25	0.20	0.21
223	44818	4.4	4.6	<0.4	0.37	0.54	0.49
218	45903	12	8.9	<2	0.5	<2	1.2
208	47881	47	53	<20	2	<20	9

[a] Calculated values are from eqs 1−3 and the simulation parameters in Table 5. [b] Experimental upper limits are given for intensities too low to be measured.

summarizes the experimental resonance Raman cross sections for the observed lines.

These spectra, dominated by a single fundamental, are qualitatively quite different from the extended overtone and combination band progressions seen in the resonance Raman spectra of other small anions such as I_3^- and NO_3^- in polar solvents,[29,31,35,36] and other triatomic molecules in solution such as SO_2 and the linear, valence-isoelectronic CS_2.[37−39] The comparison is not entirely valid because our highest excitation frequency is still well to the red of the main absorption maximum. However, these other molecules, when excited at positions on their absorption bands that roughly correspond to 208 nm in N_3^-, show much larger overtone to fundamental intensity ratios for the totally symmetric stretches than does azide. This suggests that the change in bond lengths upon electronic excitation is significantly smaller in azide than in these other systems, and/or that the coupling of the electronic transition to solvent modes is much stronger in azide, causing a faster effective electronic dephasing that preferentially reduces the intensities of overtones relative to fundamentals.[19,40]

Ab initio calculations on bare N_3^- give scaled vibrational frequencies of $\nu_1 = 1386$ cm^{-1}, $\nu_2 = 648$ cm^{-1} (doubly degenerate), and $\nu_3 = 1952$ cm^{-1}. The ground-state geometry and vibrational frequencies are nearly the same regardless of whether the additional diffuse functions are included, as these make negligible contributions to the filled orbitals. The diffuse functions do, however, have a large effect on the calculated electronic excitations. Using the standard 6-311++g** basis, the lowest dipole-allowed electronic excitation at the CIS level is a $\pi-\pi^*$ transition calculated at 51709 cm^{-1} with an oscillator strength of $f = 0.44$. The next allowed transition is $\pi-\sigma^*$ (doubly degenerate) at 55778 cm^{-1} with $f = 0.05$. The lowest calculated excitation, which has zero oscillator strength, is at 40898 cm^{-1}. Addition of the four diffuse sp shells on the nitrogen atoms results in a plethora of lower-lying excited states, all having zero or very small oscillator strengths and large contributions from the diffuse functions. The lowest of these states is at 23333 cm^{-1}, quite close to the 21614 cm^{-1} experimental electron affinity of bare N_3.[41] Evidently these calculated transitions are attempting to mimic the photoionization of N_3^-. The first significantly allowed transition is a $\pi-\pi^*$ calculated at 42396 cm^{-1} with $f = 0.16$, with a much weaker $\pi-\pi^*$ transition at 27225 cm^{-1}. The upper orbitals contributing most to the latter transition, in particular, have dominant contributions from the diffuse functions.

Corresponding calculations were carried out on complexes of N_3^- with one, three, and four water molecules. Here we focus on the structures depicted in Figures 3 and 4, which have three water molecules clustered around one end of the ion, with or without a fourth water on the other end. The initial arrangement of the first three water molecules was taken from the $[I(H_2O)_3]^-$ CTTS precursor structure of ref 5. This structure was then minimized at the Hartree−Fock level using the 6-311++g** plus diffuse basis. The four-water structure was obtained by adding the extra water to the other end of the three-water structure and reminimizing the geometry. The structures shown in Figures 3 and 4 are local minima having all-real vibrational frequencies, but we have not searched extensively for other local minima that might have lower energies.

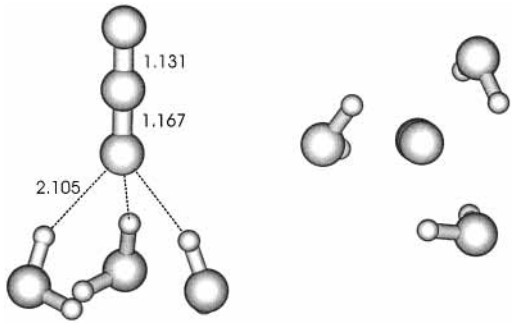

Figure 3. Two views of structure found for N_3^- with three water molecules. The N−N bond lengths and closest N···H distances (in Å) are shown; the structure has three-fold rotational symmetry.

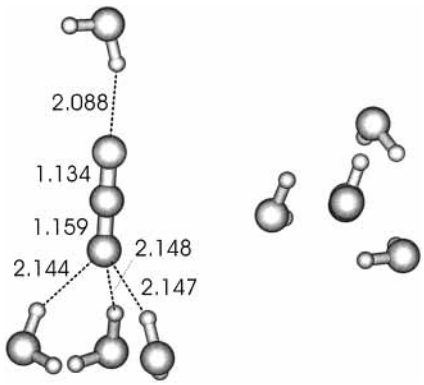

Figure 4. Two views of structure found for N_3^- with four water molecules. The N−N bond lengths and the closest N···H distances (in Å) are indicated. The structure has near-three-fold symmetry broken by the capping water.

The calculated electronic transitions of the three-water and four-water clusters are quite similar to each other and qualitatively similar to those of isolated N_3^-. Table 2 summarizes the properties of the two lowest-energy reasonably allowed transitions of bare azide and each of the two azide-water clusters. In each structure the azide ion is linear to within 1°. Both clusters have a weak transition ($f \sim 0.03$) near the energy of the observed weak shoulder in the absorption spectrum and a stronger transition ($f \sim 0.2$) near the energy of the observed strong transition in the deep-UV spectrum of aqueous azide, both polarized along the N−N−N axis. All of these transitions are dominated by excitation of an electron out of the near-degenerate HOMO and HOMO-1, which are π-type orbitals localized on the azide nitrogens. The upper orbitals involved in the lower-energy transition are mainly the highly diffuse orbitals localized on the nitrogen atoms. The upper orbitals involved in the higher-energy, stronger transition are predominantly diffuse nitrogen orbitals but also have significant contributions from basis functions centered on the water hydrogen atoms. That is, there appears to be a component of CTTS character to this transition.

Table 3 gives the calculated ground-state vibrational frequencies, excited-state displacement parameters Δ, and reorganization energies λ_v ($\lambda_v = \omega\Delta^2/2$ for harmonic modes) for the three-water cluster. What we actually calculate is the slope of the

TABLE 2: Calculated Low-Lying Electronic Transitions of N_3^-, $[N_3(H_2O)_3]^-$, and $[N_3(H_2O)_4]^-$ [a,b]

state	energy/cm^{-1}	osc. strength	excitation	CI coefficient
		N_3^-		
17	27225	0.016	10→21, 11→20	0.37
			10→26, 11→25	−0.30
40	42392	0.16	10→32, 11→31	0.46
		$[N_3(H_2O)_3]^-$		
26	39934	0.025	25→38, 26→39	−0.28, 0.28
			25→45, 26→44	−0.24
			25→39, 26→38	0.22
			25→34, 26→33	0.17
48	52162	0.20	25→***53***, 26→***52***	0.28
			25→***51***, 26→***50***	0.26
			25→***50***, 26→***51***	−0.16, 0.16
			25→45, 26→44	0.15, −0.15
		$[N_3(H_2O)_4]^-$		
26	43325	0.034	31→45	0.32
			31→50	0.30
			30→49	−0.25
			31→39	0.23
			30→43	0.21
			30→38	−0.20
			30→***44***	0.18
48	54371	0.21	30→***55***	−0.27
			31→***56***	0.27
			31→***59***	0.25
			30→***62***	−0.21
			30→49	−0.19
			30→***60***	−0.18
			31→***50***	−0.18
			30→***53***	0.17
			31→***61***	−0.16

[a] Orbitals having substantial contributions from basis functions localized on water molecules are labeled in bold italics. [b] All MOs having coefficients of at least 0.15 are listed. Energies are for the vertical transitions.

TABLE 3: Calculated Vibrational Frequencies for $[N_3(H_2O)_3]^-$ and Displacements and Reorganization Energies in the Two Lowest Strongly Allowed Excited Electronic States (Transitions 26 and 48 of Table 2)

	state 26		state 48	
ω/cm^{-1}	Δ	λ_v/cm^{-1}	Δ	λ_v/cm^{-1}
81	6.0	1434	6.0	1432
163	−4.4	1568	−4.2	1409
360	0.89	143	1.4	351
694	−0.74	191	−0.82	234
1386 (N_3^- sym. str.)	−0.28	52	−0.30	61
1622	0.43	151	0.40	129
3564	0.32	177	0.25	108

excited-state potential along the ground-state normal coordinate, which we then convert to an extrapolated dimensionless displacement assuming harmonic modes with equal ground- and excited-state frequencies.[31] Table 3 includes all vibrational modes that have reorganization energies exceeding 50 cm^{-1} in either of the excited states. The modes with the largest reorganization energies, at 81 and 163 cm^{-1}, are almost purely intermolecular vibrations involving motions of the water molecules relative to the azide ion and/or to each other. There is also significant reorganization in the intermolecular modes at 360 and 694 cm^{-1}, the in-phase combination of the three H−O−H bends at 1622 cm^{-1}, and the in-phase combination of the OH stretches hydrogen-bonded to the azide at 3564 cm^{-1}. The displacement in the azide symmetric stretch, calculated at 1386 cm^{-1}, is quite small in both electronic states.

Table 4 gives the same information for the two lowest-energy reasonably allowed electronic transitions of the four-water cluster. Here we have included only those vibrations with

TABLE 4: Calculated Vibrational Frequencies for $[N_3(H_2O)_4]^-$ and Displacements and Reorganization Energies in Two of the Lowest Strongly Allowed Excited Electronic States (Transitions 26 and 48 of Table 2)

	state 26		state 48	
ω/cm^{-1}	Δ	λ_v/cm^{-1}	Δ	λ_v/cm^{-1}
70	1.4	74	−8.4	2511
71	2.5	215	−4.1	595
77	−7.1	1965	−7.9	2401
122	−3.4	704	−3.5	747
136	−0.27	5	3.5	843
137	−0.78	41	1.1	86
166	2.4	478	2.1	376
251	0.46	26	0.68	58
345	1.0	181	1.4	357
675	−0.80	216	−0.84	236
1410 (N_3^- sym. str.)	−0.24	42	−0.27	53
1619	−0.43	152	−0.39	125
3589	−0.19	62	−0.14	36
3603	0.25	112	0.20	72

frequencies of 70 cm^{-1} or higher; this cluster has five lower-frequency modes (down to 6 cm^{-1}), some of which also have large forces upon excitation, but modeling these very low-frequency modes as undamped harmonic oscillators is highly questionable and for the purposes of our spectral modeling we prefer to lump these vibrations into the Brownian oscillator which represents the bulk solvent reorganization. Once again, the azide symmetric stretch is only weakly Franck−Condon active in both states. The dominant geometry changes involve intermolecular vibrations below 700 cm^{-1}, with smaller contributions from the bending and stretching internal vibrations of the solvating water molecules.

We use the four-water complex, which lacks any true symmetry elements, as the best (albeit not very good) model for azide in bulk water and the starting point for our spectral simulations. The computed properties of this structure were used as initial values for calculations of the UV absorption spectrum and resonance Raman intensities as described in Computational Methods under the assumption that the two observed bands correspond to transitions 26 and 48 of Table 4. Table 5 lists the electronic and vibrational parameters obtained directly from the ab initio calculations, as well as a set of refined values that better fit the observed spectra. None of the calculated vibrations of $[N_3(H_2O)_4]^-$ are clearly recognizable as predominantly the azide bend, so the parameters for the bending mode were determined purely empirically. We also made the approximation $\partial V_e/\partial q_2 = 0$ for the bending mode as it would be for linear azide, even though the presence of a very weak fundamental indicates slight symmetry breaking and a small $\partial V_e/\partial q_2$. The experimental overtone intensities are best fit with an excited-state force constant along the bending mode that is considerably smaller than that in the ground state, but not imaginary as would be expected for the excited states of bare azide (see Discussion). The "symmetric" and "antisymmetric" N−N−N stretches (the symmetry labels are inexact due to the perturbing water molecules) were assumed to have unchanged force constants upon electronic excitation, in accord with the usual observation that resonance Raman intensities are determined mainly by the slope of the upper surface at the ground-state geometry. The displacement for the symmetric stretch had to be increased considerably over the calculated values to reproduce the experimental intensities. The ab initio parameters for the azide antisymmetric stretch and for the water and intermolecular modes were not changed since there are no relevant experimental data (see Discussion). The transition moment for the upper state had to be increased somewhat to reproduce the observed strength

TABLE 5: Parameters Used in Modeling the UV Absorption Spectra and Resonance Raman Intensities of N_3^- in Water[a,b]

	lower state		upper state	
electronic properties	ab initio	refined	ab initio	refined
zero−zero energy E_0/cm^{-1}	38918	37500	45710	43300
transition length M/Å	0.269	0.24	0.596	0.86
angle between trans. moments θ/deg	−		0	90
solvent reorganization energy/cm^{-1}	−	3535	−	884
electronic line shape parameter κ	−	0.1	−	0.1
elect. inhomogeneous std. dev./cm^{-1}	−	2000	−	2000
Vibrational Properties, Azide				
ω/cm^{-1}, Δ (sym. stretch)	1410, 0.24	1343, 0.9	1410, 0.27	1343, 0.45
ω/cm^{-1}, Δ (asym. stretch)	2027, 0.081	2027, 0.081	2027, 0.050	2027, 0.050
ω_{gr}/cm^{-1}, ω_{ex}/cm^{-1} (bend)	−	640, 350	−	640, 350
Vibrational Properties, H_2O and Intermolecular				
ω/cm^{-1}, Δ	70, 1.4	70, 1.4	70, 8.4	70, 8.4
ω/cm^{-1}, Δ	71, 2.5	71, 2.5	71, 4.1	71, 4.1
ω/cm^{-1}, Δ	77, 7.1	77, 7.1	77, 7.9	77, 7.9
ω/cm^{-1}, Δ	122, 3.4	122, 3.4	122, 3.5	122, 3.5
ω/cm^{-1}, Δ	136, 0.27	136, 0.27	136, 3.5	136, 3.5
ω/cm^{-1}, Δ	137, 0.78	137, 0.78	137, 1.1	137, 1.1
ω/cm^{-1}, Δ	166, 2.4	166, 2.4	166, 2.1	166, 2.1
ω/cm^{-1}, Δ	251, 0.46	251, 0.46	251, 0.68	251, 0.68
ω/cm^{-1}, Δ	345, 1.0	345, 1.0	345, 1.4	345, 1.4
ω/cm^{-1}, Δ	675, 0.80	675, 0.80	675, 0.84	675, 0.84
ω/cm^{-1}, Δ (H−O−H bend)	1619, 0.43	1619, 0.43	1619, 0.39	1619, 0.39
ω/cm^{-1}, Δ (O−H str.)	3589, 0.19	3589, 0.19	3589, 0.14	3589, 0.14
ω/cm^{-1}, Δ (O−H str.)	3603, 0.25	3603, 0.25	3603, 0.20	3603, 0.20

[a] Parameters are defined following eqs 1−3. [b] Other parameters: temperature = 298 K, refractive index = 1.39.

of the UV absorption; the ab initio calculations do, however, predict that additional electronic transitions contribute some oscillator strength in this region of the spectrum. Finally, we could not adequately reproduce the stretching fundamental intensity in the region where both transitions contribute significantly (223 and 218 nm) unless we assumed that the two electronic transitions have perpendicular (or nearly so) polarizations. When the polarizations are parallel the contributions from the two states add destructively and produce too little intensity in this region. With so little experimental data to fit, the refined parameters given in Table 5 are neither highly accurate nor necessarily unique. They should only be considered as one set of excited-state parameters that are reasonably consistent with the available resonance Raman and UV absorption data.

5. Discussion

From a purely energetic point of view, the existence of CTTS states in this region of the UV spectrum is entirely reasonable. The photoelectron spectrum of gas-phase N_3^- yields an electron affinity of 2.68 ± 0.01 eV for N_3.[41] Small water clusters [$(H_2O)_n$, $n = 2-5$] have experimental vertical electron detachment energies that range from meV to several tenths of an eV.[42] Thus, transfer of an electron from an azide ion to a medium-sized water cluster in the gas phase should require only a little over 2 eV of excess energy, corresponding to a visible photon. Solvation may modify the energetics considerably, and there is no guarantee that an energetically allowed transition will have significant oscillator strength, but the presence of transitions with some CTTS character at 5.5−6.0 eV hardly appears surprising.

It is not clear, however, that our electronic structure calculations support true CTTS character for the low-lying transitions of aqueous azide. The CIS calculations do predict that the lowest-energy strongly allowed transition(s) of $[N_3(H_2O)_3]^-$ and $[N_3(H_2O)_4]^-$ have substantial contributions from the diffuse nitrogen-centered orbitals and the water orbitals and are not simple valence transitions of the N_3^- core. However, a true CTTS transition is usually considered to involve rapid trapping of the electron in an energetic minimum formed through the orientational polarization of a number of surrounding water molecules, a geometry that requires significant reorganization from the minimized ground-state structure.[2,7] The vertical excitations that we calculate are perhaps best considered CTTS "precursor" states, the terminology used by Chen and Sheu.[5] The calculated energy of the lowest strongly allowed ($f > 0.1$) transition of bare azide ion drops by about 9000 cm^{-1} upon adding the diffuse functions on N to the standard 6-311++g** basis, but then increases by nearly 10000 and 12000 cm^{-1}, respectively, in the three- and four-water clusters (see Table 2). This suggests that the diffuse character of this transition may be better described as a frustrated photodetachment which increases in energy with increasing confinement by surrounding water molecules. Observation of a true CTTS state would require either starting at a more favorable structure (not the ground-state minimum) or allowing the water molecules to reorient upon electronic excitation, and would probably also require more water molecules to stabilize the ejected electron. The calculations are, however, consistent with the idea that these excited states are not adequately described as pure localized valence transitions of the N_3^- core.

Further computational evidence for a CTTS-like character of these transitions comes from the calculated forces on water-localized and particularly intermolecular coordinates upon vertical excitation. In Tables 3 and 4 we have extrapolated these forces to excited-state displacements and reorganization energies assuming harmonic potentials, which is probably a poor approximation for the low-frequency intermolecular modes, but provides a useful basis for discussion. The total reorganization energy in intermolecular and water-localized modes is about 3700 cm^{-1} for the three-water cluster and even larger for both transitions of the four-water cluster. In contrast, our calculations on the strongly allowed UV transitions of two isomers of $[NO_3(H_2O)_2]^-$, which have negligible CTTS character, yielded reorganization energies of 400−900 cm^{-1} in these modes.[31]

While adding a third or fourth water molecule to the nitrate system might increase the calculated intermolecular reorganization energy somewhat, it seems clear that electronic excitation of aqueous azide produces a much larger perturbation to the surrounding solvent than does the corresponding excitation of nitrate.

The N−N bond length in gas-phase N_3^- is 1.188 Å.[43] The N_3 neutral radical in the gas phase has a bond length of 1.181 Å.[44] This comparison suggests that a true CTTS transition, involving complete removal of an electron from the azide core, should be accompanied by only a small change in the N−N bond length; 0.007 Å corresponds to a dimensionless displacement in the symmetric stretching mode of only $\Delta \approx 0.23$, remarkably close to what we obtain from the CIS calculations by extrapolating the force at the ground-state geometry to an excited-state minimum. The same qualitative conclusion is reached from the very weak Franck−Condon activity in the photoelectron spectrum of gas-phase N_3^-.[41] Also, the symmetric stretching frequency of the matrix-isolated N_3 radical (1288 cm^{-1})[45] is quite close to that of the anion. In contrast, valence transitions of triatomic molecules typically exhibit extended vibronic progressions corresponding to $\Delta \geq 2$, as seen, for example, in the UV absorption spectra of the valence-isoelectronic CS_2[38,46] and of the azide ion in thin films of KN_3.[8] The refined modeling parameters of Table 5 thus have displacements along the symmetric stretch that lie between the values expected for a valence transition of azide and for complete removal of the electron from the π HOMO. A similar conclusion is reached from the parameters for the bending mode. The $\pi \rightarrow \pi^*$ excited states of bare azide are expected to have a bent equilibrium geometry[47,48] resulting in an imaginary local frequency along this coordinate at the linear ground-state geometry, whereas the N_3 neutral radical is linear with a bending frequency of 473 cm^{-1}.[45] Our best fit to the bending mode overtone intensities is obtained with an excited-state frequency that is real, but slightly lower than that of the neutral radical. All of these results are qualitatively consistent with the resonant electronic state having a considerable degree of CTTS character, but not being a "pure" CTTS state.

While these are pleasingly consistent results, it must be pointed out that a fairly wide range of symmetric stretching displacements and excited-state bending frequencies can be about equally consistent with the experimental data. We have obtained a qualitative best fit to the data by using fairly large amounts of both "inhomogeneous" and "homogeneous" solvent-induced electronic spectral broadening. The former would arise from different local water structures that persist on time scales of picoseconds or longer, while the latter corresponds to more rapidly fluctuating structures and to the reorganization of the bulk water around the cluster in response to electronic excitation. It is reasonable to expect that both effects will be significant, but the relative importance of the two is difficult to predict and cannot be determined clearly from the experimental data. The absorption band shapes and resonance Raman intensities can be reproduced almost equally well by increasing the homogeneous (solvent reorganization) contribution, simultaneously increasing the displacements in the azide symmetric stretch and the frequency changes in the bend to compensate for the faster solvent-induced damping of the Raman amplitudes, and decreasing the inhomogeneous contribution to the broadening to maintain the overall fwhm of the absorption bands. Similarly, it is possible to decrease the solvent reorganization energy considerably while simultaneously decreasing the symmetric-stretching displacements, reducing the frequency changes in the bend, and increasing the solvent inhomogeneous broadening. A more complete data set with accurate fundamental and overtone intensities across both absorption bands would be needed to distinguish among these possibilities. However, regardless of the assumptions made about the time scale of the solvent broadening, we could not come close to fitting the available experimental data with a symmetric-stretch displacement parameter that exceeds about $\Delta = 1$ in the higher-energy state.

Our CIS calculations on the four-water cluster give a strong transition at a vertical energy of 54371 cm^{-1}. There are a number of weaker transitions at lower energies, the strongest of which is a parallel-polarized transition at 43325 cm^{-1}. Our spectral modeling, however, suggests that the intensity to the red of the strong deep-UV transition arises from states that are differently polarized. There are four transitions calculated between 46051 and 48619 cm^{-1} that have oscillator strengths in the 0.001−0.004 range and are approximately perpendicularly polarized, providing some support for the modeling results.

The ab initio calculations predict that intermolecular vibrations involving water-azide and/or water−water relative motions should be fairly strongly Franck−Condon active, as should some of the localized bending and stretching modes of the solvating water molecules. One might ask why these vibrations are not observed in the resonance Raman spectrum. The answer is that they may be, but picking them out from the broad bulk water background would be extremely difficult. The spectral simulations using the parameters of Table 5 predict that the 1619 and 3603 cm^{-1} fundamentals should be comparable in intensity to the azide symmetric stretching fundamental. However, these transitions are close to frequencies already present in bulk water and different local azide-water cluster geometries should have somewhat different frequencies, distributing the resonance enhanced intensity over a broad frequency range. Identifying these modes would require extremely careful measurement of difference spectra at a signal-to-noise ratio far exceeding what we have been able to achieve for aqueous azide. Experimental data on jet-cooled van der Waals clusters, as well as chromophores doped into crystalline or glassy solids, clearly demonstrate that intermolecular solvent−solute or solvent-localized vibrations can be strongly Franck−Condon active even in nominally solute-localized electronic transitions.[49] There is every reason to expect similar effects for chromophores solvated in bulk liquids, particularly when the electronic transition directly involves the solvent as in CTTS transitions. There have been experimental hints of resonance Raman enhancement of solvent-localized or intermolecular vibrations in liquids,[35,49−51] but no conclusive demonstration. CTTS transitions in other molecules, particularly those at longer wavelengths where better quality resonance Raman spectra can be obtained, might be good places to look for such enhancement.

Acknowledgment. This work was supported by NSF grant CHE-9708382. M.R.W. also thanks the Foundation for Research, Science and Technology of New Zealand for a New Zealand Science and Technology Postdoctoral Fellowship (Contract Number KSU-901). We thank Professor J. V. Ortiz, Olga Dolgunitcheva, and Viatcheslav Zakjevski for their generous assistance with the electronic structure calculations.

References and Notes

(1) Blandamer, M.; Fox, M. *Chem. Rev.* **1970**, *70*, 59−93.

(2) Barthel, E. R.; Martini, I. B.; Schwartz, B. J. *J. Chem. Phys.* **2000**, *112*, 9433−9444.

(3) Majumdar, D.; Kim, J.; Kim, K. S. *J. Chem. Phys.* **2000**, *112*, 101−105.
(4) Serxner, D.; Dessent, C. E. H.; Johnson, M. A. *J. Chem. Phys.* **1996**, *105*, 7231−7234.
(5) Chen, H.-Y.; Sheu, W.-S. *J. Am. Chem. Soc.* **2000**, *122*, 7534−7542.
(6) Zanni, M. T.; Frischkorn, C.; Davis, A. V.; Neumark, D. M. *J. Phys. Chem. A* **2000**, *104*, 2527−2530.
(7) Kloepfer, J. A.; Vilchiz, V. H.; Lenchenkov, V. A.; Germaine, A. C.; Bradforth, S. E. *J. Chem. Phys.* **2000**, *113*, 6288−6307.
(8) Deb, S. K. *J. Chem. Phys.* **1961**, *35*, 2122−2127.
(9) Burak, I.; Treinin, A. *J. Chem. Phys.* **1963**, *39*, 189−196.
(10) Closson, W. D.; Gray, H. B. *J. Am. Chem. Soc.* **1963**, *85*, 290.
(11) McDonald, J. R.; Rabalais, J. W.; McGlynn, S. P. *J. Chem. Phys.* **1970**, *52*, 1332−1340.
(12) Rossi, A. R.; Bartram, R. H. *J. Chem. Phys.* **1979**, *70*, 532−537.
(13) Kemmey, P. J.; Bartram, R. H.; Rossi, A. R.; Levy, P. W. *J. Chem. Phys.* **1979**, *70*, 538−540.
(14) Ferrario, M.; Klein, M. L.; McDonald, I. R. *Chem. Phys. Lett.* **1993**, *213*, 537−540.
(15) Owrutsky, J. C.; Kim, Y. R.; Li, M.; Sarisky, M. J.; Hochstrasser, R. M. *Chem. Phys. Lett.* **1991**, *184*, 368−374.
(16) Morita, A.; Kato, S. *J. Chem. Phys.* **1998**, *109*, 5511−5523.
(17) Hamm, P.; Lim, M.; Hochstrasser, R. M. *Phys. Rev. Lett.* **1998**, *81*, 5326.
(18) Dean, K. J.; Wilkinson, G. R. *J. Raman Spectrosc.* **1985**, *16*, 22−26.
(19) Myers, A. B.; Mathies, R. A. In *Biological Applications of Raman Spectroscopy;* Spiro, T. G., Ed.; Wiley & Sons: New York, 1987; Vol. 2, pp 1−58.
(20) Myers, A. B. In *Laser Techniques in Chemistry;* Myers, A. B., Rizzo, T. R., Eds.; Wiley & Sons: New York, 1995; pp 325−384.
(21) Myers, A. B. In *Advances in Multiphoton Processes and Spectroscopy;* Lin, S. H., Villaeys, A. A., Fujimura, F. Y., Eds.; World Scientific: Singapore, 1998; Vol. 11, pp 3−50.
(22) Kelley, A. M. *J. Phys. Chem. A* **1999**, *103*, 6891−6903.
(23) Williams, R. D.; Petrov, V. I.; Lu, H. P.; Hupp, J. T. *J. Phys. Chem. A* **1997**, *101*, 8070−8076.
(24) Zink, J. I.; Shin, K.-S. K. *Adv. Photochem.* **1991**, *16*, 119−214.
(25) Webb, M. A.; Kwong, C. M.; Loppnow, G. R. *J. Phys. Chem. B* **1997**, *101*, 5062−5069.
(26) McHale, J. L. *Acc. Chem. Res.* **2001**, *34*, 265−272.
(27) Lilichenko, M.; Tittelbach-Helmrich, D.; Verhoeven, J. W.; Gould, I. R.; Myers, A. B. *J. Chem. Phys.* **1998**, *109*, 10958−10969.
(28) Lilichenko, M.; Kelley, A. M. *J. Chem. Phys.* **1999**, *111*, 2345−2346.
(29) Waterland, M. R.; Kelley, A. M. *J. Chem. Phys.* **2000**, *113*, 6760−6773.
(30) Li, B.; Myers, A. B. *J. Phys. Chem.* **1990**, *94*, 4051−4054.
(31) Waterland, M. R.; Stockwell, D.; Kelley, A. M. *J. Chem. Phys.* **2001**, *114*, 6249−6258.
(32) Myers, A. B. *J. Raman Spectrosc.* **1997**, *28*, 389−401.
(33) Kulinowski, K.; Gould, I. R.; Myers, A. B. *J. Phys. Chem.* **1995**, *99*, 9017−9026.
(34) Li, B.; Johnson, A. E.; Mukamel, S.; Myers, A. B. *J. Am. Chem. Soc* **1994**, *116*, 11039−11047.
(35) Johnson, A. E.; Myers, A. B. *J. Phys. Chem.* **1996**, *100*, 7778−7788.
(36) Johnson, A. E.; Myers, A. B. *J. Chem. Phys.* **1995**, *102*, 3519−3533.
(37) Yang, T.-S.; Myers, A. B. *J. Chem. Phys.* **1991**, *95*, 6207−6217.
(38) Myers, A. B.; Li, B.; Ci, X. *J. Chem. Phys.* **1988**, *89*, 1876−1886.
(39) Myers, A. B.; Li, B. *J. Chem. Phys.* **1990**, *92*, 3310−3322.
(40) Heller, E. J.; Sundberg, R. L.; Tannor, D. *J. Phys. Chem.* **1982**, *86*, 1822−1833.
(41) Continetti, R. E.; Cyr, D. R.; Metz, R. B.; Neumark, D. M. *Chem. Phys. Lett.* **1991**, *182*, 406.
(42) Kim, J.; Suh, S. B.; Kim, K. S. *J. Chem. Phys.* **1999**, *111*, 10077−10087.
(43) Polak, M.; Gruebele, M.; Saykally, R. J. *J. Am. Chem. Soc.* **1987**, *109*, 2884−2887.
(44) Brazier, C. R.; Bernath, P. F.; Burkholder, J. B.; Howard, C. J. *J. Chem. Phys.* **1988**, *89*, 1762.
(45) Tian, R.; Facelli, J. C.; Michl, J. *J. Phys. Chem.* **1988**, *92*, 4073.
(46) Kasahara, H.; Mikami, N.; Ito, M.; Iwata, S.; Suzuki, I. *Chem. Phys.* **1984**, *86*, 173−188.
(47) Walsh, A. D. *J. Chem. Soc.* **1953**, 2301−2306.
(48) Peyerimhoff, S. D.; Buenker, R. J. *J. Chem. Phys.* **1967**, *47*, 1953−1966.
(49) Myers, A. B. *Annu. Rev. Phys. Chem.* **1998**, *49*, 267−295.
(50) Su, Y.; Tripathi, G. N. R. *Chem. Phys. Lett.* **1992**, *188*, 388−394.
(51) Veas, C.; McHale, J. L. *J. Phys. Chem.* **1990**, *94*, 2794−2800.